PHOTONICS Research

Metamaterial-based octave-wide terahertz bandpass filters

Ali Maleki,[1] Avinash Singh,[1] Ahmed Jaber,[1] Wei Cui,[1] Yongbao Xin,[2] Brian T. Sullivan,[2] Robert W. Boyd,[1,3,4] and Jean-Michel Ménard[1,*]

[1]Department of Physics, University of Ottawa, Ottawa, Ontario K1N 6N5, Canada
[2]Iridian Spectral Technologies Ltd, Ottawa, Ontario K1G 6R8, Canada
[3]School of Electrical Engineering and Computer Science, University of Ottawa, Ottawa, Ontario K1N 6N5, Canada
[4]Institute of Optics and Department of Physics and Astronomy, University of Rochester, Rochester, New York 14627, USA
*Corresponding author: jean-michel.menard@uottawa.ca

Received 8 August 2022; revised 31 January 2023; accepted 31 January 2023; posted 1 February 2023 (Doc. ID 472109); published 9 March 2023

We present octave-wide bandpass filters in the terahertz (THz) region based on bilayer-metamaterial (BLMM) structures. The passband region has a super-Gaussian shape with a maximum transmittance approaching 70% and a typical stopband rejection of 20 dB. The design is based on a metasurface consisting of a metallic square-hole array deposited on a transparent polymer, which is stacked on top of an identical metasurface with a subwavelength separation. The superimposed metasurface structures were designed using finite-difference time-domain (FDTD) simulations and fabricated using a photolithography process. Experimental characterization of these structures between 0.3 and 5.8 THz is performed with a time-domain THz spectroscopy system. Good agreement between experiment and simulation results is observed. We also demonstrated that two superimposed BLMM (2BLMM) devices increase the steepness of the roll-offs to more than 85 dB/octave and enable a superior stopband rejection approaching 40 dB while the maximum transmittance remains above 65%. This work paves the way toward new THz applications, including the detection of THz pulses centered at specific frequencies, and an enhanced time-resolved detection sensitivity toward molecular vibrations that are noise dominated by a strong, off-resonant, driving field.

https://doi.org/10.1364/PRJ.472109

1. INTRODUCTION

Sub-wavelength structures, also referred to as metamaterials, are deemed to play a crucial role for the advancement of terahertz (THz) technologies, notably in the fields of wireless communications [1,2], imaging [3], and signal processing [4]. These structures can be engineered to control several parameters of a THz pulse, such as its spectral amplitude, spatial phase, local field distribution, and polarization state [5,6]. Recently, metamaterials have been used to tune the properties of a THz pulse in both the spectral and temporal domains [7,8]. Other devices such as compact metalenses [9], chemical sensors [10], optical switching modulators [4], and perfect absorbers [11,12] were demonstrated when the metamaterial is confined to a single plane to form a metasurface. Metallic-based THz metasurfaces benefit from relatively low plasmonic loss compared to their counterparts operating in the visible or near-IR regions. More importantly, for many applications, these devices do not require precision nanofabrication tools since the metallic structures are in the range of tens of microns, scaling proportionally with the wavelength of operation, which is 300 μm (at 1 THz). The relatively large feature sizes of metasurfaces allow them to be fabricated with a scalable and cost-effective metal deposition and photolithography techniques. Moreover, metasurface devices fill a special niche for spectral filtering applications in the THz region since multilayered dielectric filters, such as those commonly used in the visible and near-IR regions, would require the deposition of millimeter-thick coatings, which is both costly and technically challenging. Previous works demonstrated that plasmonic modes in the THz region can be used to achieve tunable spectral filters [8], wide bandstops [13], and bandpass spectral filters [14]. Sharp bandpass spectral filters are especially important for signal detection since they can be used to select specific spectral components while rejecting unwanted frequencies that contribute to the noise. In standard time-resolved measurements in which all frequencies are effectively resolved simultaneously, this approach can significantly improve detection sensitivity over a given spectral region [15].

In recent years, multilayered plasmonic metasurfaces have been designed and fabricated to enable new coupled electric or magnetic modes that can contribute to creating broadband

resonances [16–18]. These filtering devices rely on two or more planar periodic arrays of subwavelength structures using different shapes such as rectangles, crosses, or circular-slot structures [13,16,17,19]. They can also include phase-changing materials, such as vanadium dioxide, to achieve tunable spectral properties [20]. The performances of such filters are typically evaluated from three main criteria: (i) the maximum transmission power within a flat passband window, (ii) the rejection efficiency of frequency components in the stopband region, and (iii) the transition between the passband and stopband regions, also referred to as the roll-off, which ultimately allows the device to distinguish desired spectral components from those nearby frequencies that must be blocked. In this paper, the broadband THz filtering properties of a bilayer metamaterial (BLMM) device are demonstrated featuring ~70% flat-top transmittance over an octave-spanning bandwidth. The stopband attenuation is greater than 10 dB over the spectral window of interest (0.3 to 5.8 THz) with some spectral regions featuring more than 20 dB attenuation. This device relies on two identical plasmonic metasurfaces, both based on a square-loop hole periodic array, separated by a transparent polymer ("coupling") layer. The BLMM design is first optimized for broadband transmission in the THz region using numerical FDTD simulations, then fabricated with standard photolithography techniques, and finally characterized using a time-domain THz system. An excellent agreement is observed between the theoretical and experimental results. In addition, it is demonstrated that stacking two BLMMs dramatically improves the rejection efficiency in the stopband region while the maximum transmittance remains relatively unaffected.

2. EXPERIMENT

Figure 1(a) shows a schematic of the BLMM broadband filters, which consist of two identical plasmonic metasurfaces separated by a thin dielectric coupling layer. A photolithography process using a negative lift-off resist to pattern the desired metasurface (square-loop hole arrays) on a 188 μm thick Zeonor substrate (Zeonor is a cyclo-olefin copolymer transparent to THz radiation with a refractive index of $n \sim 1.53$ at 1 THz). Aluminum is next deposited onto the patterned substrate using a sputtering process. It is then followed by a lift-off process that results in the desired metallic square-loop hole arrays that have a fourfold symmetry that ensures a linear optical response independent of the incident polarization state. Figures 1(b) and 1(c) show the topography of the fabricated metasurface as measured with an atomic force microscope (AFM) and an optical microscope, respectively. Depth profile analysis of the structures, as shown in Fig. 1(d), indicates a uniform aluminum thickness of ~220 nm. To create a steeper bandpass fall-off, a "double-cavity" BLMM structure is created using two identical metasurfaces (described above) in which the metasurface layers are separated by a thin dielectric coupling layer. Double-sided tapes are used as dielectric layers, which allows two metasurface devices to easily bind together. Previous work has demonstrated that the spectral properties of bilayered structures are relatively robust to misalignment between the structural elements of the stacked metasurfaces [19,21]. Nonetheless, we used a mask aligner to achieve a submicron positioning of the overlapping square-loop hole pattern to ensure good reproducibility between different samples and optimal agreement between experimental measurements and

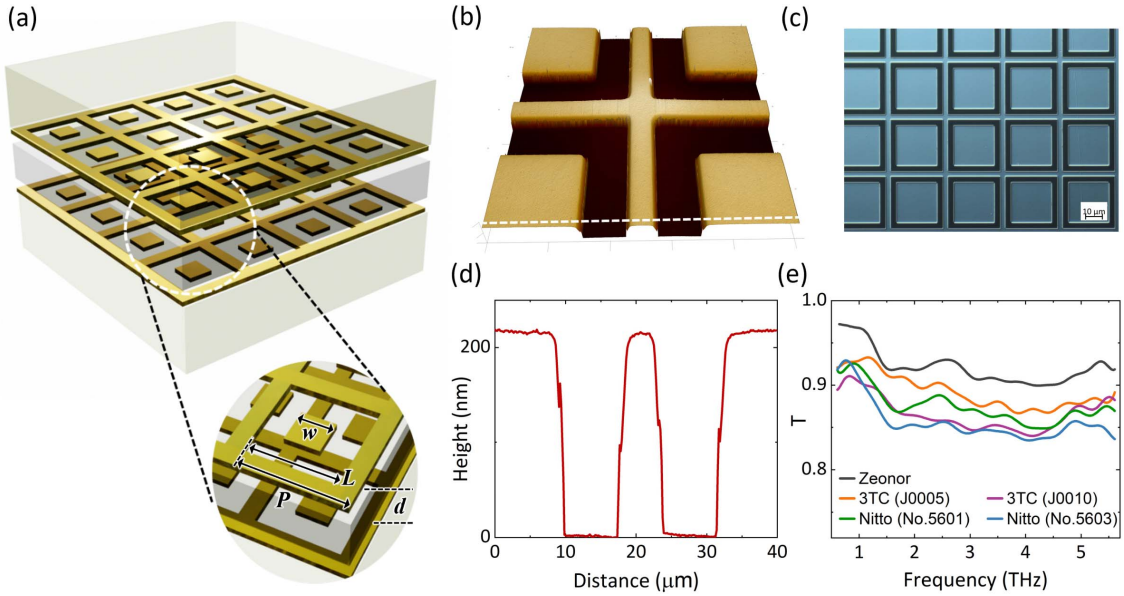

Fig. 1. (a) General schematic of the bilayer-metamaterial (BLMM) bandpass filter. Two plasmonic metasurfaces are placed adjacent to each other separated by a dielectric coupling layer of thickness d. Each metasurface consists of an array of a metallic square-loop hole structure deposited on Zeonor, a THz transparent substrate. The lattice pitch (P), length of the outer square-loop hole (L), and length of the inner square-loop hole (w) of the array are labeled with black arrows. (b) 3D atomic force microscope (AFM) image and (c) optical microscope image of the device S2, and (d) corresponding depth profile indicating a metal depth of ~220 nm. (e) THz power transmittance of the commercial double-sided adhesive tapes from Nitto and 3TC used in the fabrication of the BLMM and 2BLMM devices. In this experiment, the double-sided tapes are laminated on a Zeonor substrate and the spectral transmission measured through that substrate is also displayed (black line).

Table 1. Geometrical Parameters of the Broad Bandpass Device[a]

Device	P (μm)	L (μm)	w (μm)	d (μm)	Tape	f_0 (THz)	Δf (THz)
S1	86	80	60	33	No. 5603	0.84	0.58
S2	70	66	48	33	No. 5603	1.00	0.77
S3	52	48	36	23	J0010 and No. 5601	1.46	0.86
S4	29	23	17	10	No. 5601	3.10	1.57
S5	28	24	16	10	No. 5601	3.17	2.02
S6	32	28	15	33	No. 5603	3.44	3.20

[a]P is the lattice pitch, L is the outer square-slot length, w is the inner square-slot length, and d is the distance between two metasurfaces, as shown schematically in Fig. 1(a). The tapes used in the device fabrication are also listed as well as the center frequency (f_0) of the passband region and its spectral bandwidth (FWHM) (Δf).

numerical simulations. The tape is applied manually on the metallic side of a metasurface device while an identical device is positioned and pressed against the first one. We used different tape thicknesses to achieve optimal filtering properties at different THz regions. We are, however, limited to the thickness offered by commercial suppliers. In this work, we used tapes from Nitto Denko Corp. (Osaka) with thicknesses of 10 μm (No. 5601) and 33 μm (No. 5603), and tapes from 3TC [Taichen Corporate (Jiangxi) Co., Ltd.] with thicknesses of 9 μm (J0005) and 13 μm (J0010). Table 1 catalogs their use in the different devices presented in this work. The thickness of the tapes is measured with a profilometer (Dektak, Bruker, Billerica) and its THz absorption is characterized with time-resolved THz measurements. Figure 1(e) shows the THz spectral transmission of different tapes laminated on a Zeonor substrate as well as the one measured with the bare substrate (labeled as Zeonor).

The BLMM devices are characterized using time-domain THz spectroscopy. The experimental setup relies on an optical source delivering 60 fs pulses centered at a wavelength of 1030 nm [22,23]. Optical rectification in a 200 μm thick 110-orientated GaP crystal generates broadband THz transients detected by electro-optic sampling relying on an identical nonlinear detection crystal. Numerical simulations are performed with a 3D finite-difference time-domain (FDTD) solver (Lumerical Inc.) to investigate and optimize the target design parameters and achieve the desired broadband filtering properties in the THz region. As shown in the inset of Fig. 1(a), the geometry of the metallic structure is defined from its lattice pitch (P), length of the outer square-loop hole (L), length of the inner square-loop hole (w), and the thickness of the dielectric coupling layer (d) separating the two metasurfaces. We modeled the tape as a lossy dielectric layer with a real part and an imaginary part of the refractive index corresponding to $n = 1.65$ and $k = 0.003$, respectively, which are, within a small uncertainty, the frequency-independent values obtained with time-resolved THz spectroscopy for all tape samples. Periodic boundary conditions along the in-plane axes are employed in the simulations as well as a perfectly matched layer (PML), which is applied in the direction of optical propagation to absorb all incident fields and prevent reflection at that interface.

The geometrical dimensions shown in Table 1 were determined using numerical simulations to obtain a broad, sharp, and symmetrical bandpass region centered at different frequencies. Due to scale invariance, decreasing the size of all geometrical parameters by the same amount proportionally shifts the device's transmittance profile to shorter wavelengths (higher frequencies). The structures S1, S2, and S3 are based on a common metasurface design displaying similar ratios between geometrical parameters. As a result, these three filters display similar properties in terms of bandwidth, roll-offs, and overall transmittance profile. Limitations in the wafer-size photolithography process prevented using the same filter design at higher frequencies since defects and spatial homogeneity across the devices play a larger role as the structure parameters are decreased. More specifically, it was established that the minimum feature sizes of P–L should not be less than 4 μm. The devices S4, S5, and S6 are therefore designed using a different model to explore filtering properties centered around 3 THz, while ensuring the minimum feature is large enough to ensure the fabrication of high-quality samples. Note that the coupling parameter d cannot be fully controlled because it is based on the thickness of the adhesive region between the two metasurfaces.

3. RESULTS AND DISCUSSION

A. Spectral Filtering Performances

The metasurface geometry used for the fabrication of six BLMM devices, labelled S1 to S6, is presented in Table 1. Figures 2(a) and 2(b) show that the measured THz transmission spectrum (circles) corresponding to each structure is in good agreement with FDTD simulation results (solid lines). We find that the ratio between the highest and lowest frequencies at half the maximum of the transmittance corresponds to 2, 2.2, 1.9, 1.7, 1.9, and 2.8 for the devices S1 to S6, respectively. Therefore, the BLMM designs demonstrate an FWHM bandwidth that corresponds to approximately one octave (or a factor of 2). The transmittance spectra exhibit a super-Gaussian shape with a measured transmittance >70% in the passband region. This relatively high transmittance is partially attributable to the weak Fresnel reflection at the air–polymer interface, which is significantly lower than that typically observed at an air–semiconductor interface [8]. Additionally, the BLMM devices exhibit steep roll-offs (as measured from the high-frequency side of the passband) of >50 dB/octave and up to 100 dB/octave for S6. Such roll-off values are larger than those reported for other double-layered metamaterial devices based on structures such as skewed circular slot rings (30.2 dB/octave), meandered slots (44.6 dB/octave), and Jerusalem cross slots (58.3 dB/octave) [19]. These roll-offs are also comparable to those reported for more complex multilayered metamaterial structures [24]. As shown in Fig. 2(b) for S1, S2, and S3, such

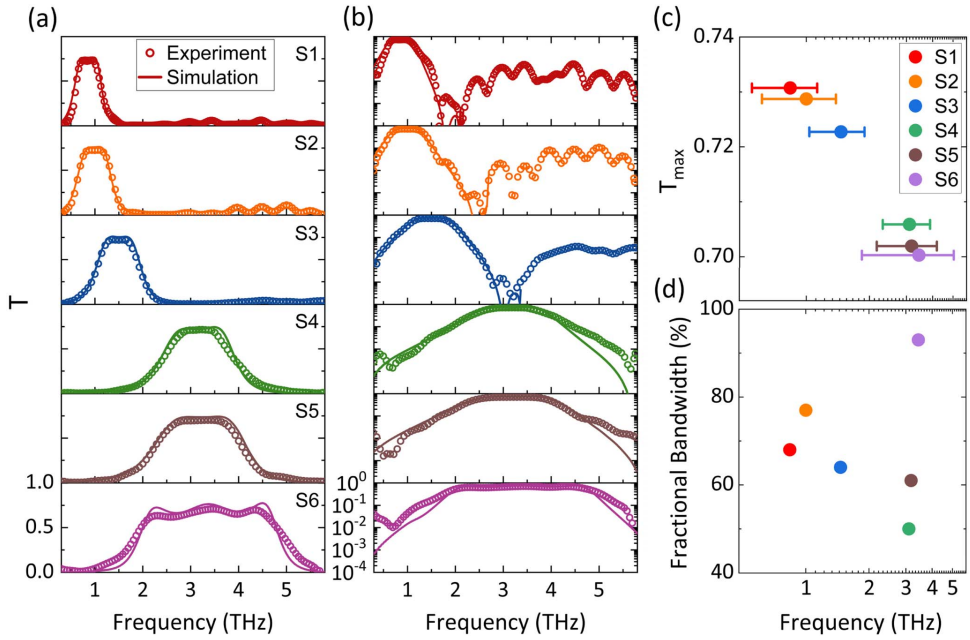

Fig. 2. THz measured (circles) and simulated (solid lines) transmittance spectrum of the BLMM-based broad bandpass filters in (a) linear scale and (b) semi-logarithmic scale. Experiments are performed with a time-domain THz spectroscopy system and are in good agreement with FDTD simulation results. (c) Measured maximum transmission (T_{max}) of the structures over center frequency in semilogarithmic scale, in which error bars present the corresponding octave-spanning FWHM linewidth. (d) Calculated fractional bandwidth (in percentage) of all BLMM devices over frequency for the experiment results.

a roll-off leads to a significant transmittance suppression, approaching 30 dB within an octave of the central transmitted frequency. Furthermore, the attenuation of these devices remains relatively high (>10 dB) at frequencies extending beyond an octave from the passband region. Figure 2(c) shows the measured maximum transmittance (T_{max}) of the six devices as a function of frequency, in which circles indicate the center frequency of the passband filters and horizontal lines correspond to the FWHM linewidth of the devices. Another figure of merit used to characterize bandpass filters is the fractional bandwidth (FBW) defined as the absolute bandwidth at FWHM divided by the central frequency. As shown in Fig. 2(d), our structures feature an FBW > 50%, and up to 93% for S6, which is, to the best of our knowledge, the largest FBW reported for a THz bandpass filter. Compared to single-layer metasurface structures, the BLMM design provides a broad bandpass region with higher attenuation in the stopband region, a flatter passband, and steeper roll-offs [25–27].

B. 3D Numerical Simulations

2D maps of the electric field spatial distribution and surface current distribution on the metallic layer of the structure S5 are shown in Fig. 3. Focusing on the spectral components within the bandpass region of the filter, Fig. 3(a) shows a

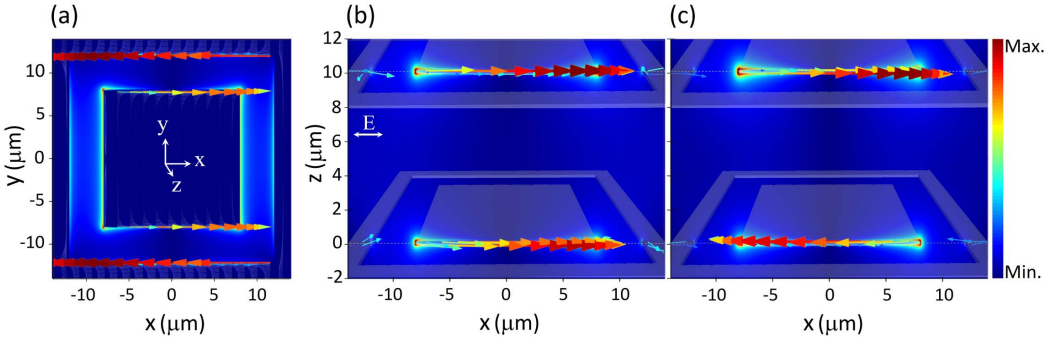

Fig. 3. Normalized electric field amplitude distribution of the BLMM structure S5. The arrows indicate surface current distribution within one period of the array. (a) Top view distribution in x–y plane at the surface of the bottom layer plasmonic structure ($z = 0.2$ μm) at the frequency of 2.9 THz. (b) and (c) Side view of the electrical field distribution and direction in the x–z plane, corresponding to a 2D cross section taken at $y = -8$ μm at a frequency of 2.9 THz and 3.6 THz, respectively. The gray 3D schematics in (b) and (c) illustrate the simulated unit cell of the stacked metasurfaces. The incident THz wave propagates in the z direction and is polarized along the x direction.

top view of the device with localized surface resonances at 2.9 THz. A field enhancement of 26 (relative to the incoming field amplitude) is observed at the corners of the central square structure along with an anisotropic field distribution with higher field amplitudes along the lateral sides of the structures due to the incident horizontal polarization. Electrical currents are induced at the outer edge of the central square and the inner edge of the surrounding frame with similar magnitude but opposite directions. Figures 3(b) and 3(c) show a cross section of the electric field amplitude and direction at frequencies of 2.9 and 3.6 THz, respectively, corresponding to the boundaries of the filter passband region. This side view is taken at the edge of the inner square structures with a 3D schematic of the unit cell (in gray) superimposed. Spectral filters relying on stacked metasurfaces are able to support effective cavity modes dominated by electric dipole resonances, magnetic dipole resonances, and standing-wave-like resonances, as previously discussed in the literature [13,16,17,19,28,29]. In Fig. 3(b), the symmetric oscillation of the induced current in the top and bottom layers indicates an electric dipole resonance. At a slightly upshifted frequency, Fig. 3(c) shows an antisymmetric resonance where electrical currents in the top and bottom layers oscillate in opposite directions. Such a mode is related to a magnetic dipolar resonance. It is the interference between these two modes, also referred to as trapped modes [29,30], that leads to such a broad and sharp passband region centered at 3.1 THz. Note that the surrounding frame creates a standing-wave-like resonance, which increases the absorption in the stopband region [16,19].

C. 2BLMM Design

To create devices with improved spectral-filtering performances, two BLMMs were joined together with a thin adhesive film (3TC-J0005) to fabricate a 2BLMM device shown schematically in Fig. 4(a). Based on the thickness of the Zeonor substrate and the adhesive film, the two BLMM structures are separated by a distance $D = 386$ μm, which is large enough to prevent near-field effects. The configuration is therefore independent of the relative cross structure alignment and orientation. We compare in Figs. 4(b) and 4(c) the THz transmittance measured with S2 and S4 as individual BLMM devices (blue curves) and the transmission measured in a 2BLMM configuration (orange curves). The 2BLMM devices show improved filtering performances in terms of the background attenuation. The stopband region, for example, provides stronger signal attenuation by approximately two orders of magnitude (dotted lines). In addition, the roll-offs (as measured from the high-frequency side) now correspond to 86 dB/octave and 85 dB/octave for S2-2BLMM and S4-2BLMM, respectively, an improvement corresponding roughly to the square value of the roll-offs measured with the corresponding BLMM devices. This stronger stopband attenuation and the sharper transitions between the passband and stopband regions are consistent with a design based on two independent BLMMs, where the transmittance spectrum then corresponds to the square transmittance of a single device. There are, however, significant advantages in stacking and binding the two BLMMs. First, the maximum transmittance in the passband region is kept relatively high (>65%) because there is no air gap, thus avoiding

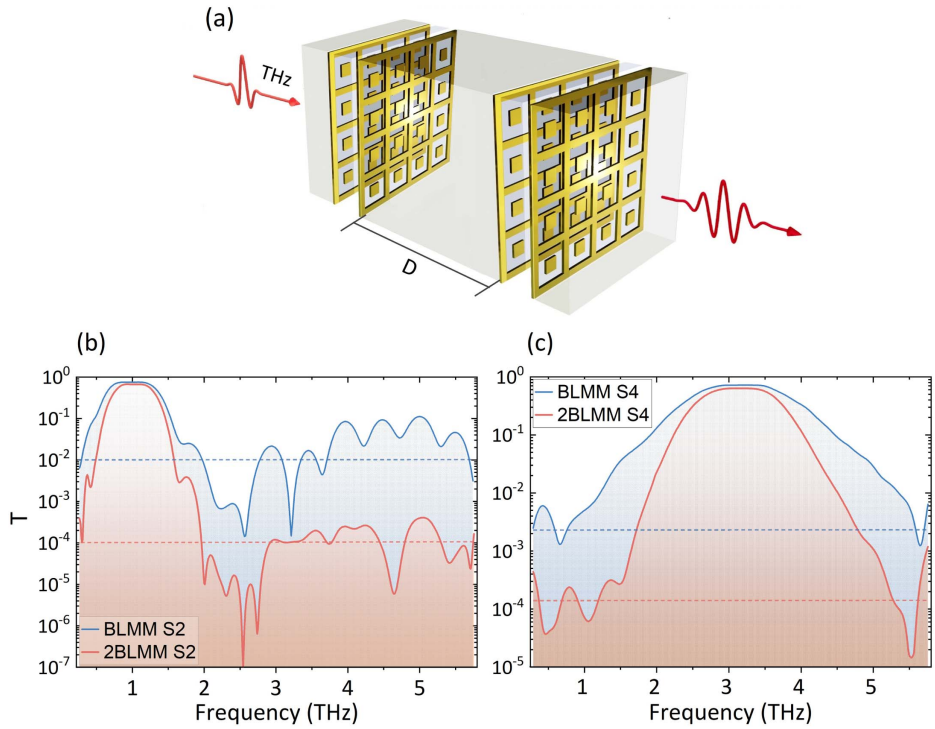

Fig. 4. (a) Schematic of the 2BLMM devices fabricated from two BLMM structures bound together with double-sided tape (separated by a length D). Comparison of the measured THz transmission of the BLMM (blue curve) and 2BLMM (orange curve) devices for (b) S2 and (c) S4. Dotted lines show the averaged attenuation floor.

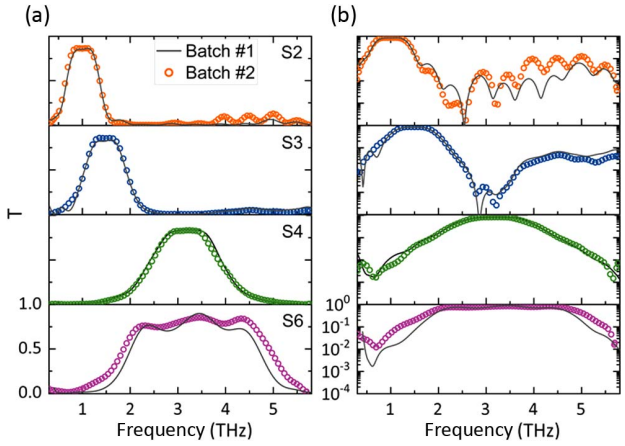

Fig. 5. Measured THz transmittance spectrum of two batches (lines and circles) of the BLMM-based broad bandpass filters in (a) linear scale and (b) semi-logarithmic scale. There is a good repeatability between the pairs of S2, S3, S4, and S6 devices fabricated in two batches and characterized on two different days.

additional Fresnel reflections. A stronger than expected attenuation also is observed in the stopband region. For S2, the transmittance between 4 and 5.5 THz is reduced from 10^{-1} to $<5 \times 10^{-4}$ (or 10 dB to 33 dB) when using a 2BLMM geometry, which exceeds the expected signal reduction based on a square dependence. This enhanced signal reduction in the stopband region may be indicative of a dipole interaction between the two BLMM devices inducing a new coupled mode that contributes to reducing transmittance across this spectral region.

D. Device Fabrication Repeatability

To test the repeatability of the fabrication process of the BLMM devices, we fabricated two sets of samples on two different days. Figure 5 shows the measured transmittance spectra for the two distinct devices based on the S2, S3, S4, and S6 designs. The pairs of S2, S3, and S4 devices are nearly indistinguishable on a linear scale [Fig. 5(a)], while a small (7%) difference in bandpass bandwidth (FWHM) can be seen for S6. This study indicates a reliable fabrication process and good repeatability. The small disparity could be due to misalignments when attaching the two metasurfaces together, or some minor variations of the metasurface structure due to the photolithography process. The S6 device is expected to be more susceptible to these variations because of its smaller feature sizes.

E. Comparison to Previous Work

We have compared the filtering performance of our devices with similar reported THz spectral filters also relying on a pair of coupled metasurfaces (see Table 2). Our BLMM and 2BLMM devices based on square hole slot metasurfaces can feature a relatively large bandpass region, sharp roll-offs, high fractional bandwidths, and a strong attenuation in the stopband region. Those are among the most critical properties of a bandpass filter. Furthermore, our design can support a bandpass centered at higher frequencies, while the structures presented in most previous work on THz filters were designed for the low frequency region (<2 THz) [16,19,21,24]. Finally, we report a stopband region extending over an unprecedentedly large spectral region. For example, device S1, which has a peak transmission around 0.9 THz, blocks spectral components between 1.5 and 6 THz, by more than 30 dB.

4. CONCLUSION

We have designed and experimentally demonstrated six bilayer metamaterial (BLMM) devices with THz bandpass filtering properties. These devices feature a flat passband region centered at different frequencies, with a maximum transmittance exceeding 70% and a large spectral bandwidth corresponding to approximately one octave. The transmittance spectrum has a super-Gaussian profile featuring steep roll-offs, while the stopband region offers a strong signal suppression (generally >20 dB) and likely extends much beyond the investigated spectral region of 0.3 to 5.8 THz. Experimental measurements and FDTD simulations are in good agreement. The fabrication of the BLMM devices is relatively straightforward because it relies on a standard photolithography process. Furthermore, it has been demonstrated that 2BLMM devices can be joined together to improve the spectral filtering selectivity. This 2BLMM configuration significantly enhances the signal suppression in the stopband region while the transmission remains flat and high (>65%). We believe this type of filter design will play a major role in selecting THz signals contained within a known spectral region to notably enable sensitive wireless communications systems [2]. In time-domain spectroscopy, spectral filtering can also lead to significant improvement of the SNR by notably blocking spectral components necessary to drive a nonlinear system while investigating the signal at higher harmonics [15].

Table 2. Performance Comparison of the Filters Presented in This Work to Similar Structures Based on Layered Metasurfaces Reported in the Literature

Study	Structure	Bandpass FWHM (THz)	Roll-off (dB/octave)	FBW (%)	Attenuation (dB)
Current designs	Square-loop hole	0.5–3.2	50–100	50–93	30–50
Ref. [19]	Skewed circular slot	0.85	30.2	51.7	~7
Ref. [19]	Meandered slots	0.45	44.6	60	~10
Ref. [19]	Jerusalem cross slots	0.45	58.3	82.2	~10
Ref. [21]	Square slot (fishnet)	0.4	–	~37	~15
Ref. [24]	Cross slot	0.69	~74	~76	30
Ref. [16]	Custom-shape slot	0.47	~65	~67	30

Funding. Natural Sciences and Engineering Research Council of Canada (RGPIN-2016-04797, STPGP/521619-2018); Canada Foundation for Innovation (35269).

Acknowledgment. The authors would like to thank Ksenia Dolgaleva and Orad Reshef for insightful discussions. Ali Maleki acknowledges support from the Ontario Graduate Scholarship (OGS), the University of Ottawa Excellence Scholarship, and the University of Ottawa International Experience Scholarship.

Disclosures. The authors declare no conflicts of interest.

Data Availability. Data underlying the results presented in this paper are not publicly available at this time but may be obtained from the authors upon reasonable request.

REFERENCES

1. H. Sarieddeen, N. Saeed, T. Y. Al-Naffouri, and M. S. Alouini, "Next generation terahertz communications: a rendezvous of sensing, imaging, and localization," IEEE Commun. Mag. **58**, 69–75 (2020).
2. Y. Ghasempour, R. Shrestha, A. Charous, E. Knightly, and D. M. Mittleman, "Single-shot link discovery for terahertz wireless networks," Nat. Commun. **11**, 2017 (2020).
3. I. E. Carranza, J. Grant, J. Gough, and D. R. S. Cumming, "Metamaterial-based terahertz imaging," IEEE Trans. Terahertz Sci. Technol. **5**, 892–901 (2015).
4. L. Wang, Y. Zhang, X. Guo, T. Chen, H. Liang, X. Hao, X. Hou, W. Kou, Y. Zhao, T. Zhou, S. Liang, and Z. Yang, "A review of THz modulators with dynamic tunable metasurfaces," Nanomaterials **9**, 965 (2019).
5. H. W. Tian, H. Y. Shen, X. G. Zhang, X. Li, W. X. Jiang, and T. J. Cui, "Terahertz metasurfaces: toward multifunctional and programmable wave manipulation," Front. Phys. **8**, 584077 (2020).
6. J. He, X. He, T. Dong, S. Wang, M. Fu, and Y. Zhang, "Recent progress and applications of terahertz metamaterials," J. Phys. D **55**, 123002 (2022).
7. L. Gingras, W. Cui, A. W. Schiff-Kearn, J.-M. Ménard, and D. G. Cooke, "Active phase control of terahertz pulses using a dynamic waveguide," Opt. Express **26**, 13876–13882 (2018).
8. L. Gingras, A. Jaber, A. Maleki, O. Reshef, K. Dolgaleva, R. W. Boyd, and J.-M. Ménard, "Ultrafast modulation of the spectral filtering properties of a THz metasurface," Opt. Express **28**, 20296–20304 (2020).
9. J. He, J. Ye, X. Wang, Q. Kan, and Y. Zhang, "A broadband terahertz ultrathin multi-focus lens," Sci. Rep. **6**, 28800 (2016).
10. S. Shen, X. Liu, Y. Shen, J. Qu, E. Pickwell-MacPherson, X. Wei, and Y. Sun, "Recent advances in the development of materials for terahertz metamaterial sensing," Adv. Opt. Mater. **10**, 2101008 (2022).
11. D. Das, K. Bhattacharyya, and S. Baruah, "A review of terahertz technology and metamaterial based electromagnetic absorber at terahertz band," ADBU J. Eng. Technol. **9**, 009020638 (2020).
12. M. Kenney, J. Grant, Y. D. Shah, I. Escorcia-Carranza, M. Humphreys, and D. R. S. Cumming, "Octave-spanning broadband absorption of terahertz light using metasurface fractal-cross absorbers," ACS Photon. **4**, 2604–2612 (2017).
13. Q. Zeng, Y. Huang, S. Zhong, T. Lin, Y. Zhong, Z. Zhang, Y. Yu, and Z. Peng, "Multiple resonances induced terahertz broadband filtering in a bilayer metamaterial," Front. Phys. **10**, 857422 (2022).
14. Y. Huang, T. Okatani, and Y. Kanamori, "Broadband stop filters for THz waves using H-shaped metamaterials with dual electronic-plasmonic functionality," Jpn. J. Appl. Phys. **61**, 1007 (2022).
15. J. C. Deinert, D. Alcaraz Iranzo, R. Pérez, X. Jia, H. A. Hafez, I. Ilyakov, N. Awari, M. Chen, M. Bawatna, A. N. Ponomaryov, S. Germanskiy, M. Bonn, F. H. L. Koppens, D. Turchinovich, M. Gensch, S. Kovalev, and K. J. Tielrooij, "Grating-graphene metamaterial as a platform for terahertz nonlinear photonics," ACS Nano **15**, 1145–1154 (2021).
16. L. J. Liang, J. Q. Yao, and X. Yan, "Ultrabroad terahertz bandpass filter based on a multiple-layered metamaterial with flexible substrates," Chin. Phys. Lett. **29**, 64–67 (2012).
17. M. Khodaee, M. Banakermani, and H. Baghban, "GaN-based metamaterial terahertz bandpass filter design: tunability and ultra-broad passband attainment," Appl. Opt. **54**, 8617–8624 (2015).
18. M. Lu, W. Li, and E. R. Brown, "Second-order bandpass terahertz filter achieved by multilayer complementary metamaterial structures," Opt. Lett. **36**, 1071–1073 (2011).
19. T.-T. Yeh, S. Genovesi, A. Monorchio, E. Prati, F. Costa, T.-Y. Huang, and T.-J. Yen, "Ultra-broad and sharp-transition bandpass terahertz filters by hybridizing multiple resonances mode in monolithic metamaterials," Opt. Express **20**, 7580–7589 (2012).
20. J. Huang, J. Li, Y. Yang, J. Li, J. Li, Y. Zhang, and J. Yao, "Active controllable bandwidth of THz metamaterial bandpass filter based on vanadium dioxide," Opt. Commun. **465**, 125616 (2020).
21. J. S. Li, Y. Li, and L. Zhang, "Terahertz bandpass filter based on frequency selective surface," IEEE Photon. Technol. Lett. **30**, 238–241 (2018).
22. A. Halpin, N. Couture, and J.-M. Ménard, "Optical pulse structuring in gas-filled hollow-core Kagomé PCF for generation and detection of phase-locked multi-THz pulses [Invited]," Opt. Mater. Express **9**, 3115 (2019).
23. W. Cui, A. W. Schiff-Kearn, E. Zhang, N. Couture, F. Tani, D. Novoa, P. S. J. Russell, and J. M. Ménard, "Broadband and tunable time-resolved THz system using argon-filled hollow-core photonic crystal fiber," APL Photon. **3**, 111301 (2018).
24. L. Liang, B. Jin, J. Wu, Y. Huang, Z. Ye, X. Huang, D. Zhou, G. Wang, X. Jia, H. Lu, L. Kang, W. Xu, J. Chen, and P. Wu, "A flexible wideband bandpass terahertz filter using multi-layer metamaterials," Appl. Phys. B **113**, 285–290 (2013).
25. D. Sun, L. Qi, and Z. Liu, "Terahertz broadband filter and electromagnetically induced transparency structure with complementary metasurface," Results Phys. **16**, 102887 (2020).
26. H. Sun, L. Zhao, J. Dai, Y. Liang, J. Guo, H. Meng, H. Liu, Q. Dai, and Z. Wei, "Broadband filter and adjustable extinction ratio modulator based on metal-graphene hybrid metamaterials," Nanomaterials **10**, 1359 (2020).
27. H.-T. Chen, J. F. O'Hara, A. J. Taylor, R. D. Averitt, C. Highstrete, M. Lee, and W. J. Padilla, "Complementary planar terahertz metamaterials," Opt. Express **15**, 1084–1095 (2007).
28. J. C. Yan, Z. K. Li, Y. Zhang, Y. L. Wang, and C. P. Huang, "Trapped-mode resonances in all-metallic metasurfaces comprising rectangular-hole dimers with broken symmetry," J. Appl. Phys. **126**, 213102 (2019).
29. O. Paul, R. Beigang, and M. Rahm, "Highly selective terahertz bandpass filters based on trapped mode excitation," Opt. Express **17**, 18590–18595 (2009).
30. V. A. Fedotov, M. Rose, S. L. Prosvirnin, N. Papasimakis, and N. I. Zheludev, "Sharp trapped-mode resonances in planar metamaterials with a broken structural symmetry," Phys. Rev. Lett. **99**, 5–8 (2007).